Effect of Mask Wall Angle on Shape Evolution during Through-Mask Electrochemical Micromachining

Effect of Mask Wall Angle on Shape Evolution during Through-Mask Electrochemical Micromachining

R. V. Shenoy* and M. Datta*

IBM T.J. Watson Research Center, Yorktown Heights, New York 10598, USA

ABSTRACT

A mathematical model to predict shape evolution during through-mask electrochemical micromachining (EMM) has been developed. Boundary element method has been used to solve the Laplace equation for electric potential with appropriate boundary conditions that describe the metal dissolution process under ohmic control. The influence of mask wall angle on shape of the evolving cavity, current distribution within the cavity and etch factor have been determined. For mask wall angles less than 90°, the etch factor increased due to the shadowing effect of the mask, whereas the etch factor decreased for mask wall angles greater than 90°. The influence of mask wall angle has been found to diminish with increasing metal film thickness.

Electrochemical micromachining (EMM) is receiving increasing attention in microfabrication for patterning, shaping, and finishing.[1] In through-mask EMM, a photoresist patterned metal workpiece is made an anode in an electrochemical cell such that the exposed metal surface is removed by high rate anodic metal dissolution. The through-mask EMM can involve etching of the metal workpiece either from a single side or from both sides simultaneously. EMM of metal films supported by insulating substrates involve single-sided through-mask metal removal. The isotropic nature of the metal removal process leads to undercutting of the mask. *A priori* knowledge of the metal removal rates and the undercutting of the photoresist is, therefore, essential in designing the photoresist mask.

In through-mask EMM, the metal dissolution takes place at the electrode surface that lies at the bottom of a cavity created by the photoresist mask. The current distribution at the electrode is thus dictated by the photoresist artwork parameters. Any variations in these parameters affects the current distribution at the metal surface and the spatial distribution of the metal removal rate. This has led to several investigations on the effect of photoresist thickness and spacing on shape evolution during through-mask EMM.[2-5] However, none of these investigations considered the variation in the mask wall angle and its influence on the shape evolution. On the other hand, small changes in exposure and development conditions during photoresist processing may lead to variations in the photoresist wall angle. These variations may lead to different current distribution at the dissolving metal surface.

Diem, *et al.*[6] investigated the influence of small variations in the wall angle on current distribution and estimated machining accuracy essential for making a recessed disk electrode. The results showed that an accuracy of 0.5° in the right angle between the insulator and the disk electrode was required to avoid any significant error in the measured current. The geometry used by Diem *et al.* is similar to that of through-mask EMM. However, in through-mask EMM, it is essential to consider the current distribution both at the initial electrode surface and within the evolving cavity.

In recent studies, the application of through-mask EMM has been demonstrated in the fabrication of several electronic components requiring different metal wall profiles. Examples include: ink jet nozzle plates containing high precision V-shaped nozzles, metal masks, cone connectors, and patterns of metal films on insulators.[7-11] The metal wall profile required for these components varied from tapered metal walls to straight metal walls. In all these studies, EMM has been demonstrated as an effective method for fabricating microelectronic components with significant cost and environmental advantages over competing fabrication technologies. For a wider application of EMM, the predictability and control of metal wall profile evolution and undercut are of particular interest. In this paper, the influence of the mask wall angle on the current distribution, the shape of the evolving cavity, and the etch factor have been investigated. The principal objective is to determine how deviations (±10°) in the mask wall angle affect the directionality of through-mask EMM.

Model Development

Figure 1 shows a scheme of the patterned electrode that has been considered for this investigation. The patterned electrode consists of a metal film of a finite thickness, b, which is partially covered with an inert photoresist mask of thickness, h. The pattern involves equally spaced straight lines of width, $2L$, that are separated by a spacing of $2a$. The angle between the photoresist sidewall and the metal electrode surface is β.

The parameters that characterize the shape evolution during through-mask EMM are (Fig. 1): (*i*) aspect ratio, h/L, (*ii*) spacing to opening ratio, a/L, (*iii*) metal film thickness ratio, b/L, and (*iv*) mask wall angle, β. The aspect ratio, spacing to opening ratio, and the mask wall angle influence the current distribution at the electrode. On the other hand, the metal film thickness ratio determines the extent to which EMM must proceed before the underlying insulator is exposed. The influence of these parameters on the undercut, U, and the etch factor are of interest. The etch factor is defined as the ratio of the maximum etched depth to the undercut, (d/U). Once the insulator is exposed, metal dissolution continues in the lateral direction leading to a change in metal wall angle, χ. Fine line through-mask EMM of metal films on insulator requires minimized undercut (hence increased etch factor), and straight walls. In this investigation, the influence of the mask wall angle, β, on the etch factor has been evaluated.

Assumptions.—The following assumptions have been made in the development of the model for shape evolution during through-mask EMM: (*i*) The shape evolution has been investigated at a patterned electrode consisting of equally spaced patterns (lines). This facilitated the use of the lines of symmetry to limit the computations to a domain defined by the electrode, the photoresist walls, the

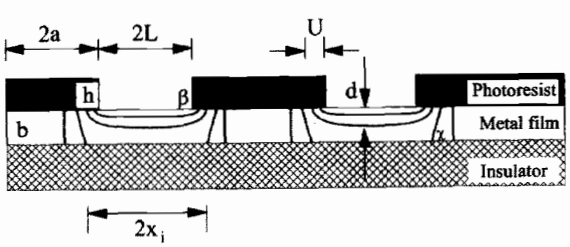

Fig. 1. Schematic diagram of a patterned metal film supported on an insulator.

* Electrochemical Society Active Member.

lines of symmetry and a virtual cathode; (*ii*) The current distribution at the metal surface has been determined solely by the ohmic effects and the electrodes were defined as equipotential surfaces. Thus, a primary current distribution has been assumed. This assumption is justified as the EMM is at relatively high current densities involving low Wagner numbers; (*iii*) Faraday's law has been used to determine the rate at which the anode surface recedes. A constant current efficiency during the EMM process has been assumed; and (*iv*) The progress of metal dissolution has been followed in terms of the ratio of the maximum etched depth and the feature half-width (d/L).

Model equations.—The current distribution has been obtained by solving the distribution of the electric potential in the electrolyte as governed by Laplace's equation

$$\nabla^2\phi = 0 \quad [1]$$

Since the kinetic resistances at the electrodes have been neglected, the boundary condition at the anode is

$$\phi = V_a \quad [2]$$

and at the cathode is

$$\phi = 0 \quad [3]$$

The potential gradients across the various lines of symmetry and insulators have been set to zero

$$\frac{\partial\phi}{\partial n} = 0 \quad [4]$$

The current distribution at the anode has been combined with Faraday's law to determine the evolution of the metal surface. The rate, r, at which the anodic surface recedes is

$$r = \frac{M\theta}{nF\rho} i \quad [5]$$

where M is the molecular weight of the metal, n is the metal dissolution valence, ρ is the density of the metal film, F is Faraday's constant, and θ is the current efficiency of metal dissolution which is assumed to be constant at 100%.

Method of solution.—Solution of the shape evolution problem requires the use of numerical techniques. The various numerical techniques available to solve the current distribution problems can be broadly divided into the domain based techniques such as finite difference and finite elements methods and the boundary based techniques such as the boundary element method. Although, finite difference method is easy to implement in regular geometries, the irregular shapes encountered in solving the shape evolution problems cannot be easily handled. The finite element method is more suitable for such problems. However, the domain based techniques require that the potential distribution over the entire domain be solved. Further, this has to be repeated at each time step to determine the shape of the evolving cavity.

The boundary element method,[12] on the other hand, has a significant advantage over the domain based techniques in solving Laplace's equation. The boundary element method can be used to determine the current distribution at the electrodes without solving the potential distribution over the entire domain. This presents a significant savings in computations in the shape evolution problems where the current distribution has to be repeatedly determined. Hence, boundary element method[12] has been used in this investigation. The current density at the anode has been determined by solving Laplace's equation, Eq. 1, and using boundary conditions, Eq. 2-4. The anode surface has then been displaced proportionally to the current density, i, using Faraday's Law (Eq. 5) to predict the shape of the evolving cavity. The details on implementation of the numerical procedure have been discussed in the Appendix.

Results and Discussion

In order to minimize the effect of the geometry other than the mask wall angle, a case of recessed electrode has been considered. For straight vertical mask walls ($\beta = 90°$) uniform current distribution is obtained for aspect ratio (h/L) of 1.0 or greater.[8] Hence, an aspect ratio of 2.5 has been chosen along with a spacing to opening ratio of 4.

Current distribution.—Figure 2 shows the normalized current distribution at the initial patterned electrode surface for various mask wall angles. For straight vertical mask walls, ($\beta = 90°$), the current distribution at the initial electrode is very uniform. However, deviation in the mask wall angle, β, from the straight vertical walls significantly alters the current distribution at the initial metal surface. For $\beta < 90°$, the normalized current density at the center of the feature is greater than 1 and it decreases as the intersection of the insulating mask and the metal electrode is approached. The current density at the intersection, for $\beta < 90°$, is equal to zero. Conversely, for $\beta > 90°$, the normalized current density at the center of the feature is less than 1 and it increases as the intersection of the insulating mask and the metal electrode is approached. The current density at the intersection, for $\beta > 90°$, is infinite. This is consistent with current distribution along an electrode near the intersection of an electrode and an insulator.

The current distribution at the initial electrode surface shown in Fig. 2 is extremely sensitive to the mask wall angle. Even small changes in the mask wall angle lead to significantly different current distributions along the electrode surface. In the following, the current distribution at various stages of the evolving cavity has been investigated.

Figure 3 shows the normalized current distribution along the evolving metal surface for a mask wall angle of 80°. The parameter, S/S_L, is a normalized distance measured from the center of the feature. The variable, S, is the the distance along the evolving metal surface measured from the center of the feature and S_L is the half-length of the evolving metal surface. The normalized arc length, S/S_L, of 1.0 corresponds to the point of intersection

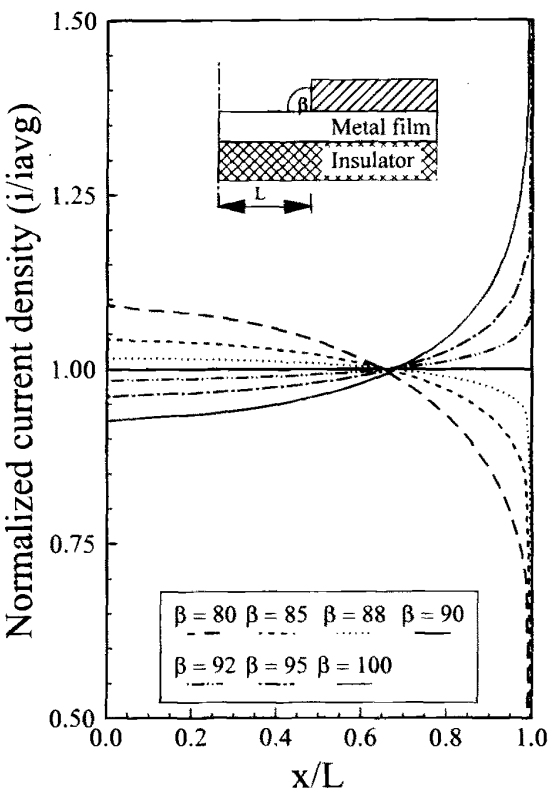

Fig. 2. Normalized current distribution at the initial metal surface for various mask wall angles, β.

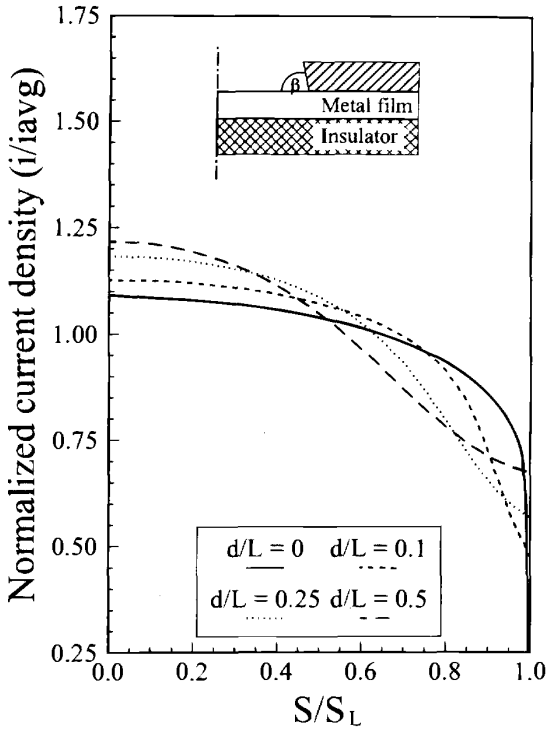

Fig. 3. Normalized current distribution along the evolving metal surface at different etched depths for mask wall angle, β = 80°.

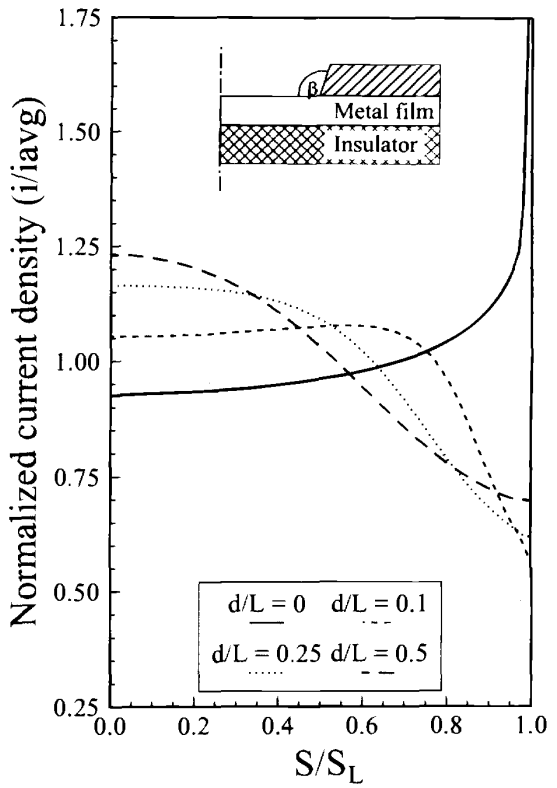

Fig. 4. Normalized current distribution along the evolving metal surface at different etched depths for mask wall angle, β = 100°.

between the metal electrode and the photoresist mask. The current distribution at the initial metal surface (d/L = 0) shows a maximum at the center of the feature and it decreases as the mask/anode edge is approached. This leads to a higher metal removal rate at the center of the feature as compared to the edge, thus providing a certain degree of anisotropy during through-mask EMM. Under strictly primary current distribution, the current density at the edge of the feature is initially zero. This would lead to no undercut as the initial metal surface is etched. However, as the metal surface recedes, the angle between mask wall and the metal surface increases. The current density at the edge becomes finite and the undercutting of the photoresist takes place.[a] The redistribution of the current density as the cavity evolves has also been shown. As the metal removal progresses, the current density at the edge becomes finite and the current distribution across the electrode becomes more uniform.

Figure 4 shows the normalized current distribution along the evolving metal surface for a mask wall angle of 100°. The maximum in the current density at the initial metal surface (d/L = 0) is at the edge of the feature. The higher current density at the edge of the feature is not desirable because it leads to higher lateral etching than that in the vertical direction. However, as the metal removal proceeds, the undercutting results in a redistribution of the current. The maximum in the current distribution begins to shift from the edge and moves toward the center of the feature. The current density at the edge becomes finite.

Shape of the evolving cavity.—Figure 5a shows the shape of the metal surface evolving for initial mask wall angles of 80°, 90° (straight vertical walls), and 100° for different amounts of etched depths. For β ≤ 90°, the maximum etched depth is always at the center of the feature.

[a] In practice, the finite resistance of the electrode kinetics would tend to smooth the initial current distribution and the undercutting would initiate even at the initial metal surface.

For β > 90°, the initial maximum etched depth is away from the center of the feature, as shown in Fig. 5b. The maximum etched depth moves toward the center of the feature as the shape evolves during EMM. An analysis of the evolving cavity shape indicates that for the same etched depth, d, the undercut depends on the mask wall angle. The undercut for mask wall angle, β = 80° is less than that for β = 90°, which in turn is less than that for β = 100°. The reduction in undercut in acute angled masks leads to higher etch factors, thus providing a certain amount of directionality in the metal removal process. In the following, the effectiveness of through-mask EMM has been further investigated in terms of the etch factor.

Etch factor.—Figure 6 shows the etch factor during through-mask EMM for an aspect ratio, (h/L), of 2.5. For masks with straight vertical walls (β = 90°), the etch factor for a recessed feature starts around 2.0 and then decreases as EMM proceeds. For mask wall angles less than 90°, the etch factor is higher than cases with straight vertical mask walls. The shadowing effect of the mask reduces the current density at the edge of the feature. Hence, the spatial distribution of the etch rate, near the edge of the feature is lower than that at the center of the feature. This reduces the undercut resulting in the increased etch factor. However, as the metal removal proceeds the difference in the etch factor between 90° and acute angled masks decreases. This is a result of the redistribution of the current within the evolving cavity that leads to the diminishing influence of the mask wall angle.

For mask wall angles greater than 90°, the etch factor is less than that for straight vertical mask walls. The current concentration near the intersection of the mask and the metal line leads to higher undercuts and lower etch factors. However, as the EMM proceeds, the difference in the etch factor for mask wall angles greater than 90° and straight vertical walls decreases. Again, the redistribution

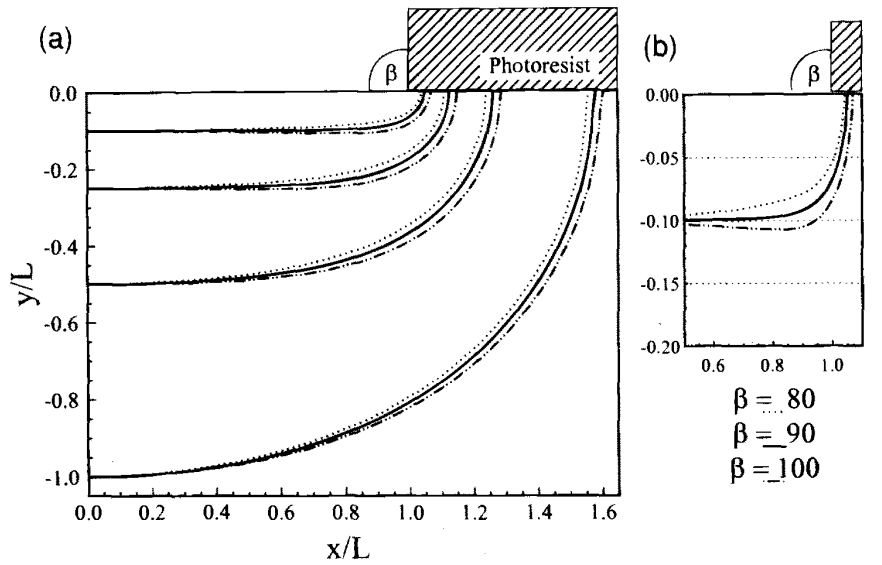

Fig. 5. (a) Shape of the evolving cavity for various mask wall angles, β; (b) the axes have been expanded to highlight the effect of mask wall angle during initial stages of metal removal.

of the current within the evolving cavity plays a role in diminishing the influence of the mask wall angle.

The discussion so far has been limited to cases where the maximum etched depth is less than the metal film thickness. In such cases, the metal removal takes place both in the vertical and the lateral directions. The degree of anisotropy is determined by the ratio of the metal removal in the two directions, *i.e.* by the etch factor. In single-sided through-mask EMM, the metal removal exposes the insulator under the metal film once the maximum etched depth exceeds the metal film thickness. In a double-sided through-mask EMM, this results in a through hole in the workpiece. In both cases, further metal removal leads to the movement of the metal surface in the lateral direction under the photoresist mask. The extent to which the metal removal is carried out then depends on the desired metal wall profile.

Metal wall profile evolution.—Figure 7 shows the evolution of the metal wall profile for a mask angle of 90°. The shape of the evolving cavity has been shown starting from the point just prior to the exposure of the insulator under the metal film. At the point where the normalized maximum etched depth (d/L) is equal to the metal film thickness ratio (b/L), the metal surface fits an elliptical curve. As the metal removal progresses, the insulator under the metal film is exposed. The metal film closer to the insulator is removed faster than that under the photoresist and the metal film profile evolves toward a straight wall. The evolution of the metal wall profile for various mask wall angles can be compared in terms of the metal wall angle, χ, which is defined as

$$\tan \chi = \frac{b}{(L + U - \chi_i)} \qquad [7]$$

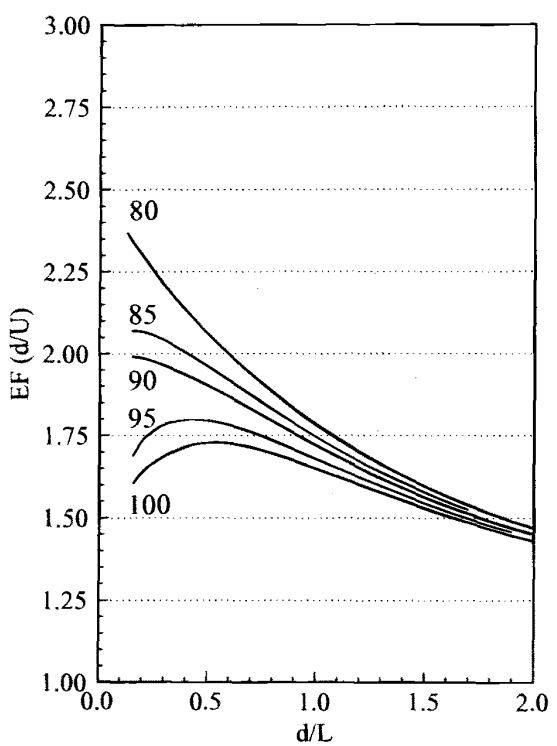

Fig. 6. Etch factor as a function of the etched depth for various mask wall angles, β.

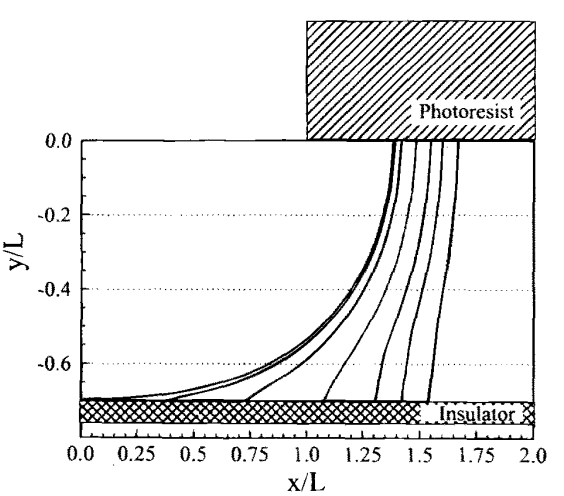

Fig. 7. Evolution of the metal wall profile after the underlying insulator is exposed.

where L is the feature half-length, U is the undercut, and x_i is the half-length of the exposed insulator. The extent of the metal removal necessary to obtain a certain metal wall angle can be expressed in terms of the ratio of undercut to metal film thickness. In the following, the influence of the mask wall angle on the metal wall angle, χ, for different metal film thickness ratios has been investigated.

Lateral metal removal in thin films ($b/L \leq 1$).— The evolution of the metal wall angle has been investigated. for metal film thickness ratio of 0.2 and 0.7. Figure 8 shows the metal wall angle as EMM progresses for a metal film thickness ratio of 0.2 and mask wall angles for 80°, 90°, and 100°. The general trend of the metal wall angle evolution for all three mask wall angles is the same. The metal wall angle is shown from the point when the bottom insulator is exposed to the point where the metal wall angle is greater than 80°. Initially, the metal wall angle, χ, increases rapidly but the rate of change of the metal wall angle decreases as the metal removal progresses. The undercut essential to obtain a desired wall profile is lower in acute angled masks than in right angled or obtuse angled masks. This indicates that the directionality of the EMM process can be improved by the use of acute angled masks when the film thickness ratio is low.

Figure 9 shows the metal wall angle as EMM progresses for a metal film thickness ratio of 0.7 and mask wall angles for 80°, 90°, and 100°. The metal wall angle evolution is similar to that observed for the metal film thickness of 0.2. Initially, the metal wall angle increases rapidly and the rate of increase slows down as the metal wall angle approaches 90° asymptotically. Figure 8 also shows that the differences in the metal wall angle for various mask wall angles are significantly less for metal film thickness ratio of 0.7, than those observed for 0.2. The influence of the mask wall angle has been shown to decrease with increasing metal film thickness.

Lateral metal removal in thick films ($b/L \geq 1$).—The influence of the mask wall angle on the etch factor is minimal as shown in Fig. 6. It is also an insignificant factor in the evolution of the metal wall profile. Thus, there are no gains to be achieved in directionality by varying the mask wall angle in through-mask EMM of thick metal films.

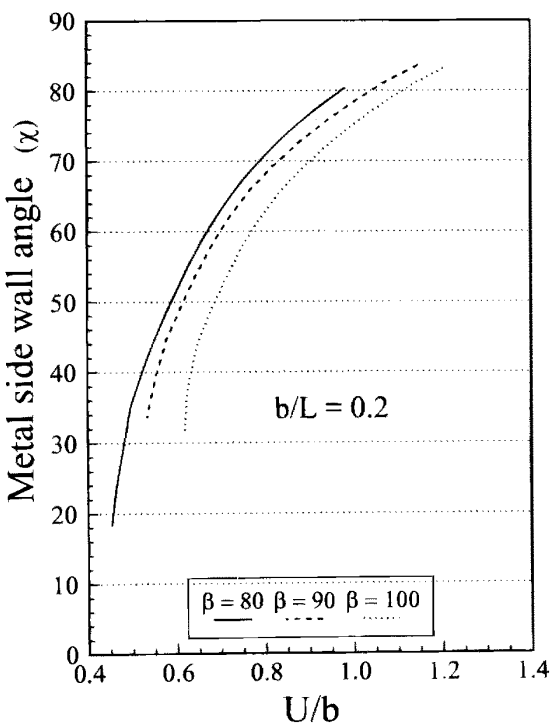

Fig. 8. Metal wall angle evolution for various mask wall angles, β for metal film thickness ratio of 0.2.

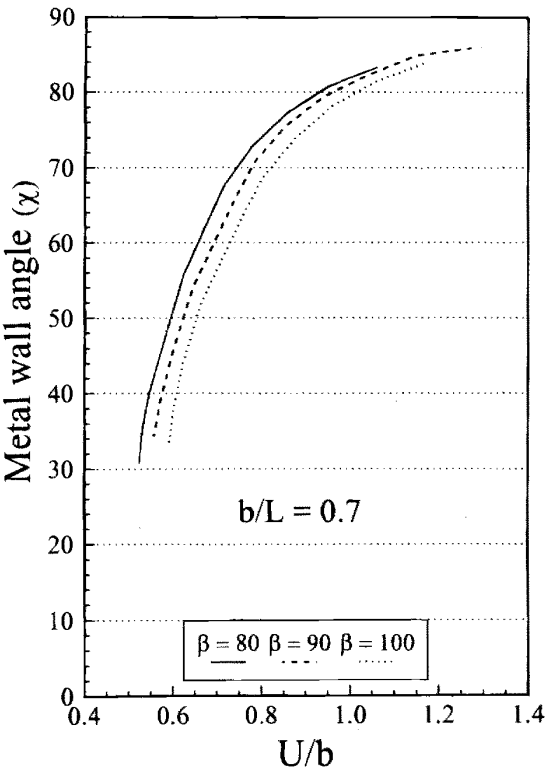

Fig. 9. Metal wall angle evolution for various mask wall angles, β for metal film thickness ratio of 0.7.

The above results can also be used to understand the influence of complex resist profiles such as a resist foot and rounded profile. The investigation of the resist foot would involve two additonal dimensionless parameters used to characterize the foot. The effect of the rounded resist profile would be important in machining of thin metal films ($b/L \leq 1$). Whereas, for thick metal films, the effect of the rounded profile would diminish with increasing metal film thickness.

The results of the present study indicate that the mask wall angle can substantially impact undercutting during through-mask EMM in early stages of metal removal. This behavior can be particularly useful in patterning of features in thin films. The photoresist mask angle of less than 90° can be used to reduce the undercut and improve the directionality of the EMM process. However, the influence of the mask wall angle diminishes with an increase in the metal film thickness ratio. This impacts the etching of deep cavities. In cases with high metal film thickness ratio, ($b/L \geq 1$), the influence of the mask wall angle is minimal.

Conclusions

The primary current distribution at the initial electrode surface is very sensitive to the mask wall angle. Even small deviations in the mask wall angle from straight vertical walls result in drastic changes in the current distribution.

During through-mask EMM, the shape of the evolving cavity causes significant redistribution of the current along the electrode surface. As the shape evolves, the current distribution becomes more uniform.

For mask wall angle of $\beta > 90°$, the current distribution at the initial surface has a maximum at the edge of the feature. The maximum in the current distribution moves

toward the center of the feature as the metal removal progresses.

For mask wall angle of $\beta < 90°$, the current distribution has a maximum at the center of the feature. As the EMM proceeds, the maximum in the current distribution remains at the center of the feature.

The mask wall angle has been shown to influence the etch factor. The influence is greatest in the initial stages of the metal removal and diminishes as the metal removal proceeds. With increasing etch depth, the etch factor for different mask wall angles approaches the etch factor for straight vertical mask walls.

Acute angled masks have been shown to improve the directionality of through-mask EMM by reducing the undercut for thin metal films. The undercut to obtain a desired metal wall profile is lower for the acute angled masks than for right angled or obtuse angled masks. However, the influence of the mask wall angle on the evolution of the metal wall profile has been shown to diminish with increasing metal film thickness ratio.

Manuscript submitted Mar. 9, 1995; revised manuscript received Oct. 1, 1995.

IBM assisted in meeting the publication costs of this article.

APPENDIX

The current distribution at the anode has been determined by solving the model equations using boundary element method.[12] The boundaries have been divided into quadratic elements by equally spaced nodes. The number of nodes have been increased till the resulting changes in the current density are negligible. This approach has been found to be sufficient to determine the current distribution for $\beta = 90°$. However, the current distribution near the anode/mask intersection has been found to change significantly as β deviates from 90°. This nonuniform current distribution problem has been solved by placing more nodes near the anode/mask intersection. The distribution of the nodes along the anode has been varied till the current density distribution near the mask/anode intersection for various values of β satisfy the the following asymptotic expression[13]

$$i(R) \propto R^{(\pi/2\beta-1)} \qquad [A\text{-}1]$$

where R is the distance from the mask/anode intersection.

At each time step, the anode surface has been displaced proportionally to the current density, i. The electrode surface at the center of the feature has been displaced vertically by a distance of 0.005-0.001 times the electrode half length, L. The time steps have been increased as the shape evolution progressed. The nodes on the newly generated surface have been repositioned. Nodes are added to maintain the initial internodal spacing. The step size used for shape evolution has been varied till the evolving profiles are independent of the step sizes.

In addition, the model has also been solved by formulating the model equations in terms of stream functions.[5] The advantage of using stream functions is that the current distributions does not show numerical instabilities near the anode/insulator edge. In the present study, the current distribution at the initial electrode surface has been determined by using stream functions whereas the current distribution on evolving surfaces have been determined by using the potential. The shape evolution and etch factors predicted by using either of the two methods (stream functions or potential) are identical.

LIST OF SYMBOLS

a	distance between photoresist edge and line of symmetry, cm
b	thickness of metallic film, cm
b/L	metal film thickness ratio
d	maximum etched depth, cm
d/L	normalized etched depth
EF	etch factor (d/U)
F	faraday constant, 96,500 C/eq
h	photoresist mask height, cm
h/L	aspect ratio
i	current density, A/cm^2
L	half-length of the feature, cm
M	molecular weight of the metal, g/mol
n	valence of metal dissolution
r	material removal rate, cm/s
R	distance from the mask/anode intersection, cm
S	distance along the evolving cavity measured from the center of the feature, cm
S_L	half-length of metal electrode in an evolving cavity, cm
U	undercut, cm
V_a	potential of the anode, V
x_i	half-length of exposed insulator, cm

Greek

β	mask wall angle, degrees
χ	metal wall angle, degrees
ϕ	potential, V
ρ	density of material, g/cm^3
θ	current efficiency of metal dissolution

REFERENCES

1. M. Datta and L. T. Romankiw, *This Journal,* **136,** 285C (1989).
2. R. V. Shenoy, M. Datta, and L. T. Romankiw, To be published.
3. R. C. Alkire and H. Deligianni, *This Journal,* **135,** 1093 (1988).
4. R. C. Alkire, H. Deligianni, and J-B. Ju, *ibid.,* **137,** 818 (1990).
5. A. C. West, C. Madore, M. Matlosz, and D. Landolt, *ibid.,* **139,** 499 (1992).
6. C. B. Diem, B. Newman, and M. E. Orazem, *ibid.,* **135,** 2524 (1988).
7. M. Datta, in *Electrochemical Microfabrication,* M. Datta, K. Sheppard, and D. Snyder, Editors, PV 92-3, p. 61, The Electrochemical Society Proceedings Series, Pennington, NJ (1992).
8. M. Datta, D. E. King, A. D. Knight, and C. J. Sambucetti, U.S. Pat. 5,105,537 (1992).
9. M. Datta and L. T. Romankiw, in *Electrochemical Technology Applications in Electronics,* L. T. Romankiw, M. Datta, T. Osaka, and Y. Yamazaki, Editors, PV 93-20, p. 123, The Electrochemical Society, Proceedings Series, Pennington, NJ (1993).
10. M. Datta, R. V. Shenoy, and L. T. Romankiw, in *ASME Symposium on Advances in Nontraditional Manufacturing Processes Research and Development,* PED-Vol. 64, Manufacturing Science and Engineering, p. 675 (1993).
11. M. Datta, in *New Trends and Approaches in Electrochemical Technology,* N. Masuko, T. Osaka, and Y. Ito, Editors, Kodansha, Tokyo (1995).
12. C. A. Brebbia and J. Dominguez, *Boundary Elements: An Introductory Course,* McGraw Hill, New York (1989).
13. A. C. West and J. S. Newman, *This Journal,* **138,** 1620 (1991).